International Journal of Environmental Sciences
ISSN: 2229-7359
Vol. 11 No. 18s, 2025
https://theaspd.com/index.php

# Effect Of Conducting Particle On Spacers In $SF_6$-$N_2$ Gas Mixture Subjected To HVAC Using Physics-Informed Neural Network (PINN) Model And Hybrid Optimization Algorithm

**Jouhar .C[1], B. Rajesh Kamath[2]**
[1]Research Scholar, Sri Siddhartha Academy of Higher Education, Tumkur, Karnataka, India
[2]Professor, Sri Siddhartha Institute of Technology, Tumkur, Karnataka, India

***Abstract***
*Insulation degradation is a major problem in the HV equipment and often causes the failure of equipment and power outages. Sulphur hexafluoride has high dielectric strength but also a high global warming potential, which means we still need an environmentally friendly alternative. A good alternative appears to be a gaseous mixture composed of 10% $SF_6$ and 90% $N_2$ for insulation preservation and environmental safety. This study investigates the breakdown voltage characteristics of solid dielectrics, specifically Polymethyl Methacrylate (PMMA) and Nylon, under high-voltage alternating current (HVAC) stress in the $SF_6$–$N_2$ environment, considering the effect of conducting particles. To enhance prediction accuracy and system intelligence, three artificial intelligence (AI)-based methodologies are integrated. A Physics-Informed Neural Network (PINN) model is implemented to embed Maxwell's equations directly into the neural network, enabling physically consistent predictions. Additionally, a hybrid optimization algorithm combining the Improved Salp Swarm Algorithm (ISSA) and Adaptive Differential Evolution (ADE) is employed to optimize spacer geometry for reduced electric field enhancement. A Graph Neural Network (GNN) is used to forecast electric field intensities and locate potential failure zones. This integrated approach significantly improves the reliability of HV insulation systems.*

***Keywords:*** *Breakdown voltage, $SF_6$–$N_2$ mixture, PMMA, Nylon, HVAC, PINN, ISSA-ADE, GNN, dielectric failure, high-voltage insulation.*

## 1. INTRODUCTION

Due to its outstanding insulation and interruption qualities, sulphur hexafluoride ($SF_6$) gas has been considered the best option for electrical power equipment since the 1960s [1]. $SF_6$ gas is one of the most extensively studied molecular gases to date due to its many industrial and scientific applications [2]. It is extensively utilized in the power sectors due to its fundamental chemical and physical characteristics, including thermal stability, nontoxicity, nonflammability, and non-explosiveness [3]. It is frequently used in gas insulated systems from several KV to the EHV class, gas blast circuit breakers, and gas insulated transmission lines [4]. $SF_6$ gas's strong electronegative properties at room temperature and at temperatures much higher than ambient are the main causes of its very high dielectric strength [5]. $SF_6$ gas has a breakdown voltage that is almost three times greater than that of atmospheric pressure air. Although $SF_6$ gas possesses exceptional electrical insulating qualities, its effects on the global environment have been hotly contested [6]. When exposed to electrical discharges, $SF_6$ gas produces extremely hazardous and corrosive substances. In addition to being an effective infrared absorber, $SF_6$ gas is not quickly extracted from the earth's atmosphere because of its chemical inertness [7]. Environmentalists have taken the role that $SF_6$ gas plays in the global greenhouse effect and ozone depletion very seriously. A number of concerns have been expressed regarding the usage of $SF_6$ gas due to its great potential for global warming [8]. It is feared that too much $SF_6$ gas will be released into the atmosphere, and the power sector naturally based its potential contribution to the greenhouse impact on estimates of future $SF_6$ gas consumption [9]. There is extremely little $SF_6$ gas produced worldwide, and it is thought to have a very limited effective impact as a greenhouse gas [10]. To reduce the amount of $SF_6$ gas used for electrical purposes, however, efforts are being made. When $SF_6$ gas bas been classified as a greenhouse gas, scientists had an even more incentive to discover a replacement [11]. To identify a replacement for $SF_6$, extensive research is being conducted. Despite the fact that gas insulated systems have been used in electric transmission systems more frequently in many nations due to their compactness, nonflammability, and high degree of dependability, the GIS's degree of compactness is severely limited by issues brought on by rising operating stresses [12]. The existence of conducting particles, which might unintentionally pollute the GIS gaps, is

one of the most significant issues with GIS [13]. Serious issues caused by metallic particles impair GIS's long-term functionality. The voltage-withstanding capacity of gas-insulated systems is diminished by these contaminated particles [14]. The introduction of additional impurities during assembly, mechanical abrasions, and vibrations brought on by load cycling can all produce these particles. It is acknowledged that particle contamination cannot be completely prevented, although it reduced to a minimum [15].
The breakdown voltage behaviour of solid dielectric materials, namely Polymethyl Methacrylate (PMMA) and Nylon, is studied under HVAC stress in an $SF_6$–$N_2$ gas mixture. The research pays specific attention to conducting particles, which can drastically affect dielectric performance. To help the research increase in accuracy and prediction ability, the research incorporates three advanced AI techniques. A first application constructs a Physics-Informed Neural Network (PINN) by embedding Maxwell's equations within the deep learning framework to allow for the prediction of breakdown voltages under various field conditions. Second, a Hybrid Optimization Algorithm, combining the Improved Salp Swarm Algorithm (ISSA) with Adaptive Differential Evolution (ADE), is used to optimize spacer geometries to reduce local electric field enhancements. Third, a Graph Neural Network (GNN) spatially maps and predicts electric field intensity across spacer surfaces, allowing for the zoning of highly probable areas for dielectric failure. These techniques form a robust simulation-driven framework for enhancing insulation reliability in high-voltage systems. The section 1 provides the introduction and the recent literatures related to the following tittle are discussed in section 2. Moreover, the section 3 provides the detail explanation about the proposed model and the section 4 deliberates the result and discussion of the proposed model. Finally, the research is concluded with the conclusion in section 5.

**1.1Objectives in this study**

- To investigate the breakdown voltage behaviour of solid dielectrics (PMMA and Nylon) under HVAC stress in an $SF_6$–$N_2$ gas mixture, particularly in the presence of conducting particles that influence dielectric strength and failure mechanisms.
- To develop a Physics-Informed Neural Network (PINN) model that integrates Maxwell's equations for accurately predicting breakdown voltages in complex dielectric environments under varying electrical stress conditions.
- To design and implement a Hybrid Optimization Algorithm (ISSA–ADE) for optimizing spacer geometry, aiming to reduce electric field distortion and enhance the dielectric performance of insulating components.
- To utilize a Graph Neural Network (GNN) for mapping and forecasting electric field intensity on spacer surfaces, enabling the identification and visualization of high-risk zones prone to dielectric failure.

## 2. LITERATURE REVIEW

In 2021 Amanulla et al. [16] developed using various ratios of the $N_2$:$SF_6$ gas mixture, the flashover characteristics at AC voltages were thoroughly analysed and characterized. This work has looked at the effects of floating particles, the usage of several insulating spacers, including PMMA, PP, and NYLON, and their combination to generate hybrid spacers in relation to the non-uniform electric field (needle-plane) electrode arrangement. The N2:SF6 gas mixture has been used to study the surface flashover capabilities of individual and hybrid spacers. In 2021 Fan et al. [17] proposed c-C4F8 and N2 ternary gas mixtures with CF3I by considering the process of surface discharge streamer production. Using COMSOL, a surface discharge model in a CF3I gas mixture under DC voltage bas been produced. By solving the drift-diffusion equations of particles, the discharge process has been demonstrated. This produced, among other factors, the changes in electric field and particle concentration during the development of the streamer. The theoretical underpinnings for a reliable partial discharge diagnosis are provided by these findings. Therefore, the model's particle, streamer, and streamer branch properties are contrasted with those of models for two more different gases. In 2023 Ahmed et al. [18] investigated the influence of charges accumulated on the inner surfaces of the void on the electric field distribution between the spacer's exterior and interior surfaces, considering their placement within the insulator at different sizes. This effect becomes more noticeable when the radius is 2 mm and the inner surface of the vacuum has a charge density of 1 (μC/m2). In 2022 Meer et al. [19] focused on the features of breakdown under such overvoltage in relation to standard operating voltages, the study examined the mechanisms and conditions that led to electrical failure. A stepped leader propagation strategy is known to regulate

the GIS breakdown process under compressed SF6 gas. Despite the fact that several researchers have carried out a range of experimental experiments for various experimental settings under DC, AC, or impulsive high voltages alone, there is currently no systematic way to anticipate or approximate the

| Author & Citation | Aim | Methodology | Problem Statement | Research Gap |
|---|---|---|---|---|
| Amanulla et al. (2021) [16] | To analyse flashover characteristics of various N2:SF6 ratios with different spacers | Experimental study using needle-plane electrodes; insulating spacers (PMMA, PP, NYLON) and hybrids | Lack of clarity on how hybrid spacers affect flashover in non-uniform fields | No AI/mathematical model used; dynamic behavior under different voltage waveforms unaddressed |
| Fan et al. (2021) [17] | To model surface streamer discharge in CF3I mixtures under DC | COMSOL model solving drift-diffusion equations | Limited understanding of CF3I gas mixture discharge dynamics | Does not evaluate AC conditions or include experimental validation |
| Ahmed et al. (2023) [18] | To study how void surface charges influence internal E-field distribution | Simulation of voids in insulators with varying radii and positions | Electric field distortion by voids is not well understood | Real-world validation and varying material properties not considered |
| Meer et al. (2022) [19] | To explore breakdown features in GIS under overvoltage | Literature review and experimental insights | No systematic modelling exists for GIS under superimposed over voltages | Lacks numerical modelling and AI prediction framework |
| Dong Li et al. (2022) [20] | To fabricate UV-curable coatings with high flashover voltage | Material synthesis with BaTiO3 nanoparticles + acrylic resin | Traditional coatings show poor adhesion and complex processing | Effect under long-term AC/DC stress and different environmental conditions not tested |
| Wang et al. (2022) [21] | To mitigate E-field near triple junction and spacer surface | Topology optimization, simulation of field distributions | E-field enhancements cause premature failure in GIS | Real-time operational testing and dynamic stress analysis absent |
| Wang et al. (2022) [22] | To assess DC flashover in SF6/CF4 gas combinations | Two electrode systems with differing field uniformities | Flashover compromises insulator reliability | Lack of investigation into temporal degradation and surface tracking behavior |
| Duan et al. (2025) [23] | To evaluate surface charge in GIS insulator under AC | Experimental study on scaled model with metal particles | Surface charge influenced by gas type and particle location | Limited to fixed time interval; doesn't analyze transient behavior |
| Wang et al. (2023) [24] | To simulate epoxy degradation under reactive gas particles | Molecular dynamics simulations using force fields | SF6 byproducts cause severe insulation erosion | Simulation limited to idealized particles; ignores mechanical stresses and thermal effects |

| | | | | |
|---|---|---|---|---|
| Wang et al. (2021) [25] | To examine charge accumulation under different gas environments | Real-size epoxy insulator with Kelvin probe under DC | Different gases affect surface charging behaviour | Does not include impulse voltage effect or AI-based pattern recognition |

breakdown voltages of the GIS under such overlaid conditions.

In 2022 Dong Li et al. [20] developed as a rapid and simple method for fabricating SFGM, the UV-curable coating demonstrated strong adhesion to the epoxy matrix, high flashover voltage, and ease of processing. Utilizing the coating material's rheological and photocuring characteristics, the component formula and UV-curing method which included mixing photocurable acrylic resin with BaTiO3 (BT) nanoparticles coated with perfluoro-silane were optimized. In 2022 Wang et al. [21] designed to enhance the dispersion of E fields close to the triple junction area and along the spacer surface. The analysis focused on how design factors affected the resulting electric field mitigation degree and field distributions. E field mitigation results and structure processability were balanced by using the appropriate design parameter values. In 2022 Wang et al. [22] proposed surface flashover quality of the combination were evaluated, as flashover frequently occurred at the insulator contact, compromising the equipment's ability to operate safely; therefore, epoxy resin composites were used for solid insulators. Through the development of two distinct electrode systems with varying electric field uniformities, the characteristics of DC flashover are investigated. The results demonstrate that the flashover voltage in the 20% SF6/80% CF4 combination bas been over 70% of the SF6 value at the same pressure.

In 2025 Duan et al. [23] proposed the use of air (80% $N_2$ / 20% $O_2$) as an alternative insulating gas based on its environmental benefits and acceptable dielectric performance and C4F7N/CO2 mixes, a linear metal particle connected to the HV electrode on the convex surface of a down-scaled 252k VC GIS basin insulator model bas been used to analyse the surface charge behaviour. Charge densities on both surfaces were measured, after applying a 40 kV AC voltage for five minutes, and the effects of the metal particle and gas properties were investigated.

In 2023 Wang et al. [24] focused on using force field molecular dynamic modelling techniques, the chemical reaction kinetics of epoxy polymer under the effect of very energetic particles were investigated in order to elucidate the degradation process. For damage caused by S particles, the outcomes were similar.

In 2021 Wang et al. [25] focused on how the charge accumulation pattern on a real-size epoxy insulator with a multiarc surface profile depends on gaseous ionization using various gas atmospheres. A system of coaxial electrodes bas been created in order to examine the charging behaviour at dc voltages of -10, -20, and -30 kV. The Table 1 denotes the problem statement.

**Table 1: Problem statement**

## 3. METHODOLOGY

The methodology adopted integrates an experimental approach with AI-based prediction to study the breakdown voltage characteristics of solid dielectrics, Polymethyl Methacrylate (PMMA) and Nylon under HVAC stress, within the gas mixture of 10% $SF_6$ and 90% $N_2$, when conductive particles are in the system. The experimental setup uses a needle-plane electrode arrangement to produce non-uniform electric fields are apply controlled breakdown testing. For predictive analysis, a Physics-Informed Neural Network (PINN) is developed, wherein Maxwell's equations are embedded directly into the network architecture to provide an accurate prediction of dielectric breakdown behaviour. A Hybrid Optimization Algorithm that integrate with Improved Salp Swarm Algorithm combined with Adaptive Differential Evolution (ADE) optimizes the spacer geometry that reduces concentration of the electric field. The GNN in turn models the electric field intensity distribution over the dielectric surfaces and predicts the high-risk zones of failure. This multi-layered framework allows for very accurate modelling and improvement of the insulation system performance.

### 3.1Experimental Setup

This experimental setup Figure 1 and Figure 2 has been arranged for studying the breakdown voltage behaviour of Polymethyl Methacrylate and Nylon under difficult conditions of HVAC in the tested environment given by 10% $SF_6$ gas and 90% $N_2$ gas mixture. Using needle-to-plane electrodes, a non-

uniform field is created in an attempt to simulate actual insulation conditions. The samples are held between the electrodes in a sealed high-pressure test chamber that allows precise control of gas composition and pressure. Conducting particles such as metallic dust were introduced to simulate contamination scenarios and to study any possible influence on dielectric behaviour. The electrodes were connected to a high-voltage power supply that could be slowly increased in voltage, while breakdown has been detected using a digital storage oscilloscope and voltage divider circuit. The tests were repeated several times for the same conditions to confirm the consistency of measurements, keeping temperature and humidity within certain limits to reduce outside influence on the results.

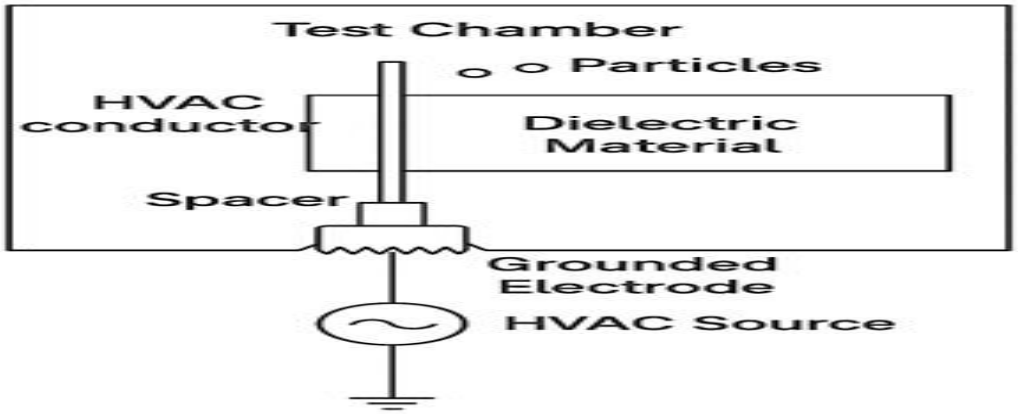


**Figure 1: Experimental Setup**

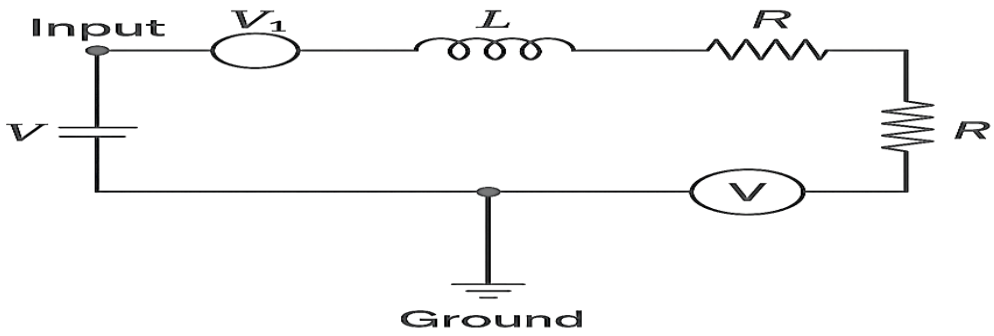


**Figure 2: Circuit Diagram of HVAC**

**3.2 System Architecture: AI-Assisted HV Insulation Design Framework**

**3.2.1 Objective:**

To design a reliable and environmentally safer HV insulation system using an AI-integrated framework that:

- Predicts breakdown voltage under HVAC stress.
- Optimizes spacer geometry to reduce electric field concentration.
- Forecasts electric field distribution and identifies potential failure zones.

The proposed system model integrates advanced artificial intelligence techniques with physical principles to enhance the reliability and environmental compatibility of high-voltage (HV) insulation systems using an $SF_6$–$N_2$ gas mixture. The process begins with the definition of key input parameters, including the type of dielectric material (PMMA and Nylon), the gas mixture composition (10% $SF_6$ and 90% $N_2$), the nature of applied high-voltage alternating current (HVAC) stress, and the presence of conducting particles that may influence breakdown characteristics. These inputs serve as the foundation for the Physics-Informed Neural Network (PINN), which is employed to predict the breakdown voltage distribution across the dielectric surface. Unlike conventional neural networks, the PINN incorporates Maxwell's equations directly into its learning process, ensuring that all predictions adhere to the governing physical laws of electromagnetism. This enables the model to deliver highly accurate and physically consistent

estimations of electric stress regions within the insulation system. Overall Architecture shown in Figure 3.

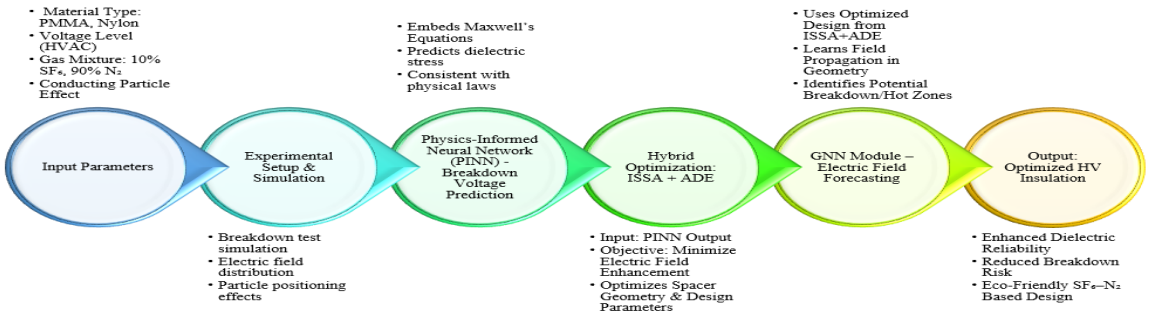


**Figure 3: Proposed Architecture**

Following the PINN-based predictions, a hybrid optimization algorithm that combines the Improved Salp Swarm Algorithm (ISSA) and Adaptive Differential Evolution (ADE) is applied. This module receives the predicted voltage distribution from the PINN and focuses on optimizing the geometry and positioning of insulation spacers. The objective is to minimize electric field enhancements and ensure uniform stress distribution, thereby increasing the dielectric strength and operational lifespan of the HV equipment. The optimization process iteratively adjusts the design configuration to achieve the most efficient and reliable performance under the given HVAC conditions.

Once the geometry has been optimized, a Graph Neural Network (GNN) is deployed to further analyse the spatial characteristics of the electric field. By representing the dielectric structure as a graph where nodes correspond to specific points in the material and edges represent the spatial or physical relationships the GNN learns how electric fields propagate throughout the system. This enables the accurate forecasting of electric field intensities and the identification of potential failure zones or hotspots. The GNN thus serves as a final predictive layer that ensures the optimized design not only performs well theoretically but also remains robust under practical stress scenarios. Figure 4 shows the overview study model. Multi-stage system comprising PINN for breakdown voltage prediction, ISSA-ADE for geometry optimization, and GNN for electric field forecasting forms a comprehensive, intelligent framework. It not only enhances the insulation performance but also supports environmental sustainability by enabling the use of reduced $SF_6$ concentrations without compromising system reliability.

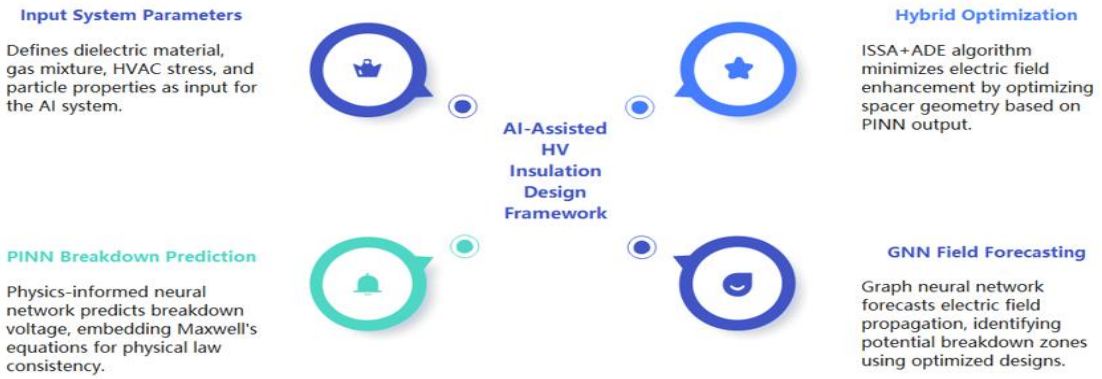


**Figure 4: Overview of the study**

### 3.3Input Layer

The input layer of the proposed system model encapsulates all critical physical and environmental parameters required to simulate and analyze the breakdown behavior of HV insulation systems. Two solid dielectric materials Polymethyl Methacrylate (PMMA) and Nylon are selected due to their distinct dielectric and mechanical properties. PMMA is a transparent thermoplastic with a relative permittivity (dielectric constant) typically in the range of 2.6–3.6, high surface resistivity (~$10^{14}$ Ω·cm), and excellent arc resistance, making it suitable for applications requiring transparency and good insulating

characteristics. It exhibits brittle behavior under mechanical stress but maintains stability under high electric fields. Nylon, on the other hand, is a semi-crystalline polyamide with a dielectric constant around 3.5–4.0, moderate surface resistivity (~$10^{12}$ Ω·cm), and good mechanical strength and flexibility. It is known for its resilience in harsh environments, making it a reliable material for insulation under mechanical vibrations and thermal cycling.

The gas environment comprises a gaseous mixture of 10% Sulphur Hexafluoride ($SF_6$) and 90% nitrogen ($N_2$). $SF_6$ is traditionally used in HV systems due to its exceptionally high dielectric strength (approximately 2.5 times higher than air) and strong electronegativity, which helps to absorb free electrons and suppress electrical discharges. $SF_6$ has a global warming potential (GWP) of 23,500, making it an environmental concern. To mitigate this, its concentration is reduced and supplemented with nitrogen, which is inert, eco-friendly, and cost-effective. The $SF_6$–$N_2$ mixture retains sufficient insulation capability while significantly reducing the environmental footprint. Table 2 presents the dielectric properties of the materials used in the study.

**Table 2: Dielectric Material Properties**

| Property | PMMA (Polymethyl Methacrylate) | Nylon (Polyamide) |
|---|---|---|
| Relative Permittivity (εr) | 2.6 – 3.6 | 3.5 – 4.0 |
| Surface Resistivity | ~$10^{14}$ Ω·cm | ~$10^{12}$ Ω·cm |
| Dielectric Strength | 15 – 25 kV/mm | 14 – 22 kV/mm |
| Volume Resistivity | ~$10^{14}$ Ω·cm | ~$10^{13}$ Ω·cm |
| Thermal Conductivity | ~0.19 W/m·K | ~0.25 W/m·K |
| Mechanical Strength | Brittle under high stress | Tough and flexible |
| Moisture Absorption | Very Low | Moderate |
| Application Suitability | Transparent, rigid insulators | High vibration environments |

The dielectric system is subjected to high-voltage alternating current (HVAC) stress, which is representative of real-world operational conditions encountered in substations, circuit breakers, and gas-insulated switchgear (GIS). HVAC stress introduces dynamic electric fields that can challenge the dielectric endurance of materials, especially under long-term exposure. To replicate realistic fault-prone conditions, conducting particles are introduced into the system model. These particles may originate from manufacturing defects, loose metal fragments, or contamination and are known to act as field intensifiers due to their sharp edges and high conductivity. The size, shape, material (e.g., aluminium, copper, or steel), and spatial position of these particles significantly influence the local electric field enhancement factor (EF). Even a small particle can create a localized electric field peak several times higher than the average field, leading to partial discharge inception and eventual breakdown. Tables 3 and 4 summarize the characteristics of the 10% $SF_6$ + 90% $N_2$ gas mixture and the parameters of the conducting particles, respectively.

**Table 3: Gas Mixture Characteristics (10% $SF_6$ + 90% $N_2$)**

| Parameter | $SF_6$ | $N_2$ | Mixture (10% $SF_6$ + 90% $N_2$) |
|---|---|---|---|
| Dielectric Strength (relative) | ~2.5× air | ~1× air | ~1.6–1.8× air |
| Global Warming Potential (GWP) | 23,500 | ~0 | Significantly reduced |
| Breakdown Voltage (per mm gap) | ~89 kV (at 1 atm, 1 cm) | ~30–35 kV | ~55–60 kV |
| Toxicity | Non-toxic | Non-toxic | Non-toxic |
| Electronegative? | Yes | No | Moderately electronegative |
| Arc Quenching Ability | Excellent | Poor | Improved (vs. $N_2$ alone) |
| Cost | High | Low | Medium |

**Table 4: Conducting Particle Parameters**

| Parameter | Description |
|---|---|
| Material Types | Aluminum, Copper, Steel, Dust Contaminants |
| Shape | Spherical, Needle-like, Irregular |
| Size Range | 0.1 mm – 5 mm |
| Electrical Conductivity | High ($10^6$ – $10^8$ S/m depending on material) |
| Position Sensitivity | Critical (near electrodes/spacers increases EF dramatically) |
| Effect on Electric Field (EF) | Enhances local EF by 2× to 10× depending on proximity |
| Risk Contribution | Initiates partial discharges, accelerates dielectric aging |
| Consideration in Model | Randomized spatial insertion during simulation for robustness |

By considering these comprehensive parameters—dielectric material properties, environmentally safe gas mixture characteristics, realistic AC stress conditions, and particle-induced field distortions the input layer ensures that the downstream AI models (PINN, ISSA-ADE, GNN) are trained and optimized on data that closely mimic the physical behavior of actual HV insulation systems. This provides a reliable and generalizable framework for predictive modelling and insulation system optimization.

**3.4 Phase 1: Physics-Informed Neural Network (PINN) – Breakdown Voltage Prediction**

Partially differential equations (PDEs) used to characterize PINN, a family of universal function approximators that integrates knowledge of any physical rules controlling a particular data set into the learning process (Eqn 1). Some biological and technical challenges have limited data availability, which reduces the resilience of traditional machine learning models utilized in these applications. Prior knowledge of general physical principles serves as a regularization agent during neural network (NN) training, reducing the range of acceptable solutions and enhancing the function approximation's generalizability.

There are often two parts to the loss function of a physics-informed neural network:

$$L_{total} = L_{data} + \lambda L_{physiscs} \quad (1)$$

$L_{data}$ be the Supervised learning loss (e.g., Mean Squared Error) from labelled breakdown voltage data, $L_{physiscs}$ has been denoted as Loss due to the residual of the governing physical equations, $\lambda$ denoted weighting factor to balance the two losses.

Electric and magnetic fields behave fundamentally as described by Maxwell's equations. For dielectric breakdown studies in electrostatic conditions, the appropriate Maxwell equation (Eqn 2) reduces to Gauss's law for electricity:

$$\nabla . E = \frac{\rho}{\varepsilon} \quad (2)$$

The relationship between electric field and potential is shown in Eqn (3):

$$E = -\nabla V \quad (3)$$

The Poisson's equation (4):

$$\nabla . (\epsilon \nabla V) = -\rho \quad (4)$$

Where $V$ be the Electric potential, $\varepsilon$ be the Permittivity of the material (can vary spatially), $\rho$ denoted as Free charge density.

This equation governs the distribution of the electric potential in the dielectric medium and is needed to model the electric field behaviour that leads to breakdown.

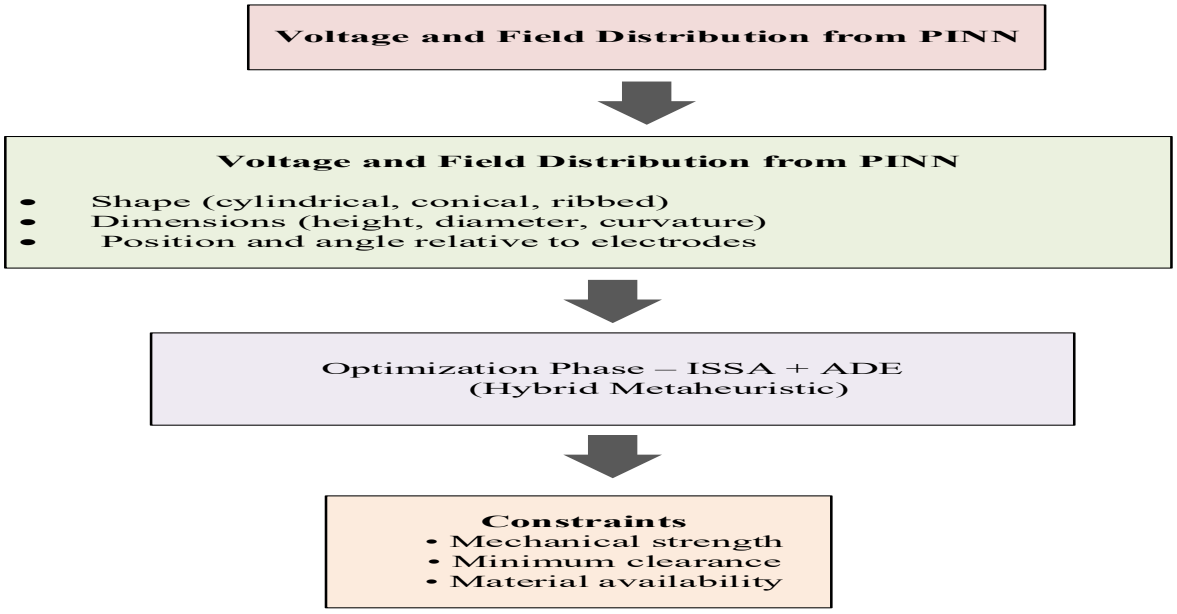


**Figure 5: Optimization Workflow for Spacer Design in High-Voltage Insulation Systems**

**• PINN-Maxwell Framework for Breakdown Voltage Prediction**

In order to accurately predict breakdown voltages, a hybrid model is created that utilizes the training of the neural network by embedding Maxwell's Poisson equation in the training. The network learns an electric potential field $\hat{V}(x)$ which maximizes the fit to the observations of the data while satisfying the governing physics is shown in Eqn (5):

$$L_{total} = \frac{1}{N_d}\sum_{i=1}^{N_d}\left(\hat{V}(x_i) - V_i\right)^2 + \lambda.\frac{1}{N_p}\sum_{j=1}^{N_p}\left(\nabla.\left(\varepsilon\nabla\hat{V}(x_j)\right) + \rho_j\right)^2 \quad (5)$$

Where:

$\hat{V}(x)$ denoted as Electric potential predicted by the PINN, $N_d$ denoted as Number of labelled data points, $N_p$ denoted as Number of collocation points, $x_i$ , $x_j$ Spatial coordinates, $\rho_j$ denoted as Charge density at location $x_i$ , $x_j$, $\lambda$ denoted as Weighting coefficient between data and physics losses.

With this hybrid PINN-Maxwell model, the neural network honours both the training data as well as the physics, enabling it to predict a dielectric breakdown voltage consistently with high accuracy from a physics-informed perspective. Figure 6 illustrates the hybrid optimization process of spacer design using ISSA–ADE and PINN-based field analysis.

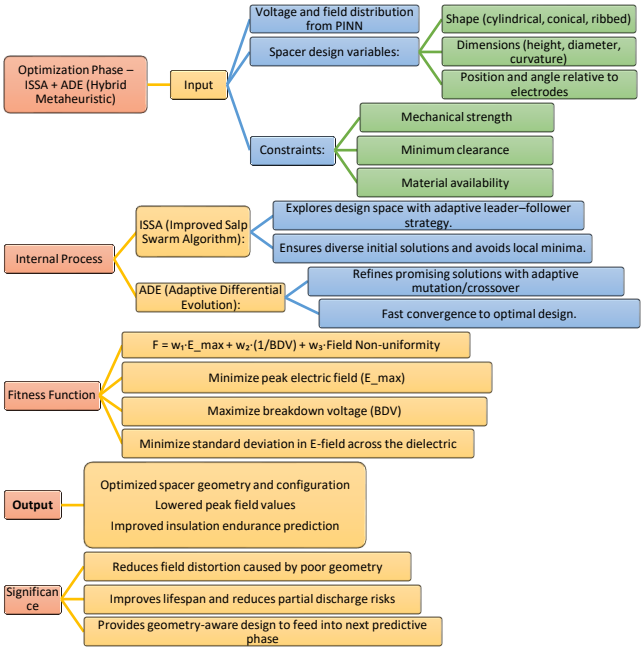


**Figure 6: Hybrid Optimization of Spacer Design Using ISSA–ADE and PINN**

### 3.5Phase 2: Optimization Phase –Salp Swarm Adaptive Differential Optimization

SSA is suggested by mimicking the deep-sea salps swarming tendencies. In their natural habitat, salps typically behave in a chain-like, unique swarming manner to improve their mobility and foraging through quick, coordinated alterations. The population of SSA is therefore divided into two classes leaders and followers in order to replicate the salps chain behaviour. The food source directs the leaders, who then direct the followers' movements.

#### 3.5.1 Initialization of population

as demonstrated by Equation (6), the salp population is shown as a $N \times D$ -dimensional matrix named $Y_{N,D}$. Let's further assume that the optimization issue is directed towards a prey called $F$. Next, the SSA population is initialized at random using Equation (7):

$$Y_{N,D} = \begin{bmatrix} y_{1,1} & y_{1,2} & \cdots & y_{1,D} \\ y_{2,1} & y_{2,2} & \cdots & y_{2,D} \\ \vdots & \vdots & \ddots & \vdots \\ y_{N,1} & y_{N,2} & \cdots & y_{N,D} \end{bmatrix} \quad (6)$$

$$Y_{N,D} = \text{rand}(N, D) \times (ub - lb) \quad (7)$$

where $Y_{N,D}$ includes $N$ salps' population data with dimensions $D$, $\text{rand}(N, D)$ represents a $N \times D$-dimensional matrix created by using a random function, $ub$ signifies the search space's upper bound, while lb denotes its lower bound.

#### 3.5.2 Fitness function

Minimization of voltage breakdown error in Physics-Informed Neural Network are shown in Eqn (8).

$$L_{data} = \frac{1}{N}\sum_{i=1}^{N}\left(V_{pred}^{(i)} - V_{pred}^{(i)}\right)^2 \quad (8)$$

$V_{pred}$ predicted breakdown voltage from the PINN, $V_{true}$ experimentally observed breakdown voltage.

#### 3.5.3 Dynamic Weight

SSA can balance the shift from global exploration to local exploitation by employing a control parameter called $d_1$. Consequently, $d_1$ is sometimes referred to as a transition parameter. By observing Equation (9), the result indicates that $d_1$ adopts a nonlinear model and that, as the number of repeats increases, From the constant 2, it attenuates adaptively. The method starts to use the local area to obtain a precise estimate when the transition parameter is less than one; when it is greater than one, the algorithm carries out global exploration to find the target search area. The transition value $d_1$ employed in the standard SSA, however, is not very appropriate for the method, as we discovered after using the mapping mutation procedure for followers. Consequently, the precise expression for the adjusted transition parameter $d_1$ is as follows:

$$d_1 = a \times 3^{-\left(\frac{b \times l}{l_{max}}\right)^2} \quad (9)$$

where $a\ (\text{default} = 2)$ and $b\ (\text{default} = 5)$ are constants. Furthermore, the approach with the altered transition parameter and the mapping mutation operation is called IMOSSA.

Despite the advancements in SSA, as mentioned earlier, in many cases, additional precise nonlinear modifications are still required to prevent the locally optimum solution. In light of this, this study proposes to adaptively modify the transition parameter $d_1$ by employing a nonlinear dynamic weight that is represented in particle swarm optimization after the inertia weight. The dynamic weight is as follows:

$$\omega = \omega_{max} - (\omega_{max} - \omega_{min}) \times \left(\frac{l}{l_{max}}\right)^{(1/2)} \quad (10)$$

where $\omega_{max}$ and $\omega_{min}$ are represented as the dynamic weight's upper and lower bounds, respectively. Additionally, max = 1 and min = 0.0001 are constant values. Therefore, the following is how equations (9) and (10), which explain the improved position update of leaders, work:

$$Y_{i,j} = \begin{cases} F_j + \omega . d_1 \left(d_2 + lb_j(ub_j - lb_j)\right), & d_3 \geq 0.5 \\ F_j - \omega . d_1 \left(d_2 + lb_j(ub_j - lb_j)\right), & d_3 < 0.5 \end{cases} \quad (11)$$

According to the dynamic weight approach, the algorithm's dynamic weight is higher at the beginning of the search and boosts its capacity for global exploration; later on, it is lower and intensifies the algorithm's capacity for local exploitation. The improved technique accelerates convergence and improves the transition impact from exploration to exploitation by precisely controlling the fine-tuned transition parameter $c_1$ once more.

### 3.5.4 Mapping Mutation Operation for Followers

Using Equation (11) to update their current location, followers in the SSA demonstrate a typical Newtonian movement. However, this kind of movement also produces a small number of adherents and a population that lacks diversity. Therefore, the mapping mutation process used in MOSSA, the upgraded SSA, is provided by

$$Y_{i,j}^{l+1} = \begin{cases} Y_{i,j}^{l} \times \left(1 + G(\beta)\right), & d_4 \geq 0.5 \\ lb_j + \beta \times \left(ub_j - lb_j\right), & d_4 < 0.5 \end{cases} \quad (12)$$

where a random number from the [0,1] border is denoted by $d_4$ . Gaussian variation is likewise focused on finding a small region around the original individual $\beta$ is $G(\beta)$, as the normal distribution's properties show, assuming that the probability density of the continuous random variable is constant. A stochastic number generated by the Tent chaotic map is formula (12) $G(\beta)$, which is a Gaussian mutation operation. To adjust the appropriate population size during mutation function dynamically we use Adaptive Differential Evaluation.

A fitness landscape-based adaptive population size strategy is suggested to dynamically modify the ideal population size. For population size adaptation, the LSHADE recommended linear population size reduction (LPSR) scheme has shown to be an excellent plan, as everyone is aware. However, the LPSR process does not adapt to the changing landscape of objective functions; instead, it just drops linearly as the number of assessments grows. For this reason, we suggested the fitness landscape-based adaptive population size scheme (FL-APS). Equation (13) provides the specifics of the suggested mechanism:

$$N_{G+1}^{FL} = \text{round}\left[\left(N^{init} - N^{min}\right) \times \varphi + N^{min}\right] \quad (13)$$

Equation (13) used to modify the FL-APS once a balance between population size and generation number has been established with the addition of a FES.

### 3.5.5 RFDB Selection Method

Rotulet Fitness-Distance Balance-Based (RFDB) selection is used to increase its exploitation capabilities. Every individual's distance and fitness levels are taken into account throughout the RFDB selection process. The values of fitness and distance will thus influence people's decisions. One argues that the RFDB selection procedure is unfair in this case. The global optimal solution found by using the roulette wheel method to identify the high-potential solution candidate. Below is an explanation of the specifics of the RFDB selection procedure. Calculate the distance

$$D_{pi} = \sqrt{\left(y_{[i,1]} - y_{[best,1]}\right)^2 + \left(y_{[i,2]} - y_{[best,2]}\right)^2 + \cdots + \left(y_{[i,D]} - y_{[best,D]}\right)^2} \quad (14)$$

Form the distance vector

$$D_p \equiv \begin{bmatrix} d_1 \\ . \\ . \\ . \\ d_m \end{bmatrix} \quad (15)$$

Calculate each person's score according to their fitness and distance statistics.

$$S_{pi} = F \times normf_i + (1 - F) \times normD_{pi} \quad (16)$$

The normalized values of its ness and distance for the its person,

Form the RFDB score vector

$$S_p \equiv \begin{bmatrix} s_1 \\ . \\ . \\ . \\ s_N \end{bmatrix} \quad (17)$$

Based on the score vector, a candidate is chosen at random using the roulette wheel selection method. This person is engaged to produce a new position using Equation (17).

When the RFDB selection method is used to choose an individual candidate from the population with $X_{RFDB}$.

### 3.5.6 Small-Hole Imaging Reverse Learning Strategy

The problem that the majority of intelligent optimization algorithms have with local extremes is addressed by the reverse learning technique. This strategy's basic idea is to use population optimization to develop

a comparable reverse solution for the present solution. Then, choose the best choice by comparing the objective function values of the two possibilities before moving on to the next iteration. This approach is used in the paper to propose a small-hole image diversity learning strategy to enhance population diversity, increase the algorithm's ability to search globally, and make it more similar to the global optimal solution. The principle of small-hole imaging, Equation (18)

$$\frac{\left(\frac{a_j-b_j}{2}\right)-Y_{best}}{Y'_{best}-\frac{(a_j-b_j)}{2}}=\frac{h}{h^1} \qquad (18)$$

Let $\frac{h}{h'}$. The equation is Equation (19) when $X'$ best is achieved by the transformation, and Equation (18) is obtained when n=1.

$$Y'_{best}=\frac{(a_j+b_j)}{2}+\frac{(a_j+b_j)}{2n}-\frac{Y_{best}}{n} \qquad (19)$$

$$Y'_{best}=(a_j+b_j)-Y_{best} \qquad (20)$$

Equation (19) demonstrates that when $n=1$, small-hole imaging reverse learning is the appropriate general reverse learning technique. However, at the moment, small-hole imaging learning only uses general reverse learning to obtain a fixed reverse point, which is frequently far from the global optimal position.

$$Y_i=\begin{cases}Y_i^{Salp}, F_i^{Salp}<F_i\\ Y_i, \quad F_i^{Salp}\geq F_i\end{cases} \qquad (21)$$

Since the fitness value had increased in the new location, it has been argued that the population had relocated to a more practical area close to its original site.

### 3.5.7 Termination

Return the optimized salp position $Y_{best}$ after checking the stopping condition. This optimized salp yields the minimum voltage breakdown error in the PINN model. End the algorithm once convergence criteria or maximum iterations are met.

Figure 7 illustrates the proposed work that integrates an improved Salp Swarm Algorithm (ISSA) with Adaptive Differential Evolution (ADE). This hybrid optimization approach is designed to minimize the voltage breakdown error in Physics-Informed Neural Networks (PINNs). The process involves dynamic parameter updates, leader–follower position adjustments, and reverse learning to obtain the optimal salp solution

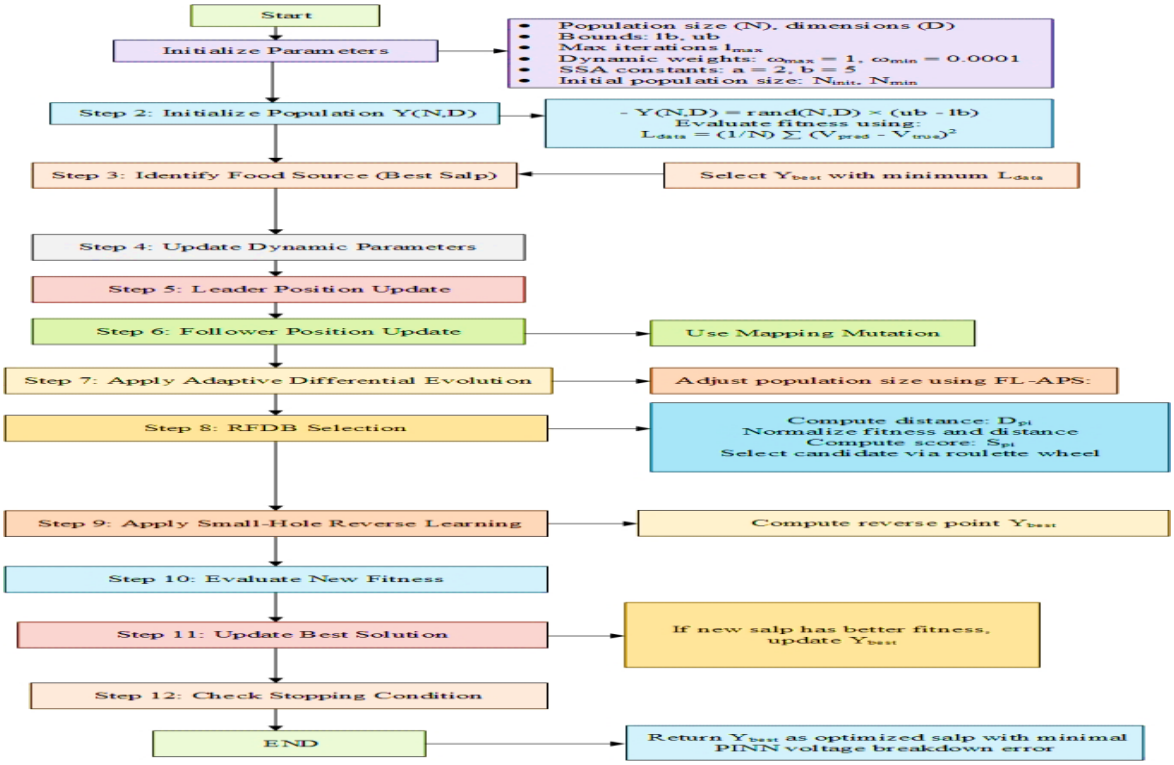


**Figure 7: Proposed work**

### 3.6 Phase 3: Graph Neural Network (GNN) – Electric Field Forecasting & Failure Zone Localization

GNN provide an advanced way to model electric field intensities that are spatially distributed over complex geometries of insulation, such as gas-insulated system spacer surfaces. From this point of view, discretization of an insulating region into a graph structure occurs with nodes conceptualized as discrete points on the spacer surface, whereas edges have their physics defined. Each node $v_i \in \mathcal{V}$is associated with a feature vector $h_i^{(0)}$that encodes initial physical parameters, such as permittivity, geometry, or electric potential. The GNN propagates information across the graph using message passing and aggregation mechanisms defined by Eqn (22):

$$h_i^{(k+1)} = \sigma\left(\sum_{j\in\mathcal{N}(i)} \emptyset\left(h_i^{(k)}, h_j^{(k)}, e_{i,j}\right)\right) \quad (22)$$

where $h_i^{(k)}$ is the node embedding at the $k-th$ layer, $N(i)$ denotes the set of neighbors of node $i$, $e_{i,j}$ represents edge features, $\phi$ is a learnable message function, and $\sigma$ is a nonlinear activation function.

GNN captures complex spatial interactions and field gradients, enabling the prediction of electric field intensity $E_i$ at each node. The final output can be mapped in Eqn (23):

$$E_i = f_{readout}\left(h_i^{(K)}\right) \quad (23)$$

where $f_{readout}$ is a fully connected layer or regression head applied after K GNN layers.

GNN-based framework can precisely locate areas of high stresses conducive to dielectric failure and so increases predictive reliability without exhaustive finite element simulations. It thus supports rapid design iterations and monitoring of insulation health in vivo in high-voltage systems, thereby creating operational safety for the system.

## 4 Result & Discussion

This results section covers the prediction of breakdown voltage, Proposed Salp Swarm Adaptive Differential Evolution (SSADE) algorithm, and the GNN framework. The approach captures intricate dielectric behaviour and field distribution, enabling finer estimations of breakdown voltage. On comparison with other methodologies, the one proposed here is defined by improved predictive power and sturdiness, endorsing the excellence and reliability of the suggested hybrid framework.

**Table 5: Breakdown voltage Comparison Table**

| Metric | Proposed | Conventional ANN | SVR | Random Forest | GPR |
|---|---|---|---|---|---|
| MAE (kV) | 1.42 | 3.27 | 2.95 | 2.1 | 1.95 |
| RMSE (kV) | 1.88 | 4.91 | 4.26 | 3.01 | 2.85 |
| MSE (kV²) | 3.53 | 24.11 | 18.14 | 9.06 | 8.12 |
| MAPE (%) | 2.10% | 7.60% | 6.90% | 4.30% | 3.70% |
| sMAPE (%) | 2.00% | 7.10% | 6.30% | 4.00% | 3.40% |
| $R^2$ Score | 0.983 | 0.872 | 0.894 | 0.931 | 0.943 |
| Relative Error (%) | 2.50% | 6.80% | 5.90% | 4.20% | 3.80% |
| MedAE (kV) | 1.21 | 2.91 | 2.5 | 1.85 | 1.71 |
| Max Abs Error (kV) | 3.65 | 8.44 | 7.13 | 4.79 | 4.22 |
| NRMSE (%) | 2.00% | 6.30% | 5.70% | 3.90% | 3.60% |
| MBE (kV) | 0.12 | 1.25 | 1.1 | 0.65 | 0.48 |

### 4.3Breakdown voltage Comparison

In this comparison, multiple error metrics were analysed to evaluate model performance are shown in Fig 5. These include Mean Absolute Error (MAE), Root Mean Square Error (RMSE), Mean Squared Error (MSE), Mean Absolute Percentage Error (MAPE), Symmetric Mean Absolute Percentage Error (sMAPE), Coefficient of Determination ($R^2$), Relative Error, Median Absolute Error (MedAE), Maximum Absolute Error (Max Abs Error), Normalized RMSE (NRMSE), and Mean Bias Error (MBE). These metrics comprehensively assess the accuracy, consistency, and bias of breakdown voltage prediction models.

#### 4.1.1 Mean Absolute Error

MAE quantifies the average magnitude of prediction errors without considering their direction. The lower the value, the more accurate the prediction. The proposed model yields the lowest MAE of 1.42 kV compared with 3.27 kV of Conventional ANN, 2.95 kV of SVR, 2.1 kV of Random Forest, and 1.95 kV of GPR. This substantial decrease in error shows how robust the model is to capture the breakdown voltage patterns more accurately rather than leads to over- or underestimation of breakdown voltage in isolated cases. With nearly a 57% improvement over the second-best GPR model, the method in question is perfect for sensitive electrical insulation systems where accuracy is paramount. In high-voltage engineering, a smaller MAE hence has to be provided to enhance the reliability of predictions while also reducing the risk during component design. Thusly, in the context of MAE, the model's capabilities are an indication of its efficiency and applicability in the realm of precise breakdown voltage estimation.

#### 4.1.2 Root Mean Square Error (RMSE)

RMSE assesses the square root of the average of squared differences between predicted and actual values. It penalizes higher errors with weights, makin' it suitable for systems where any big variation can be a risk. The proposed model obtained the lowest RMSE of 1.88 kV against models like ANN (4.91 kV), SVR (4.26 kV), Random Forest (3.01 kV), and GPR (2.85 kV) for larger errors along with insulation reliability analysis. RMSE being more sensitive to outliers shows that the proposed model avoids extreme errors in prediction, which is great compared to the traditional AI models. The proposed framework, compared with the GPR model, shows an improvement of almost 34%, which substantiates its applicability in real high-voltage insulation scenarios. Fewer high-impact errors confirm that the model learned truly complex patterns involved in breakdown voltage prediction.

#### 4.1.3 Mean Squared Error (MSE)

Mean of the square of differences between actual and predicted values, with the larger errors being penalized really more because of the square. In the proposed model, the MSE is only 3.53 kV squared, which basically suggests that it is the best compared to others: a simple ANN with 24.11 kV squared MSE, SVR with 18.14 kV squared MSE, Random Forest with 9.06 kV squared MSE, and GPR with 8.12 kV squared MSE. This sharp diminution, with more than a 56% reduction over the GPR, underlines the ability of the model to eliminate virtually large portions of errors that could considerably affect the overall reliability of prediction. Because high voltage insulation systems need exact and consistency the intention is to minimize MSE to prevent failure of the systems, and this excellent MSE performance to minimize risk allows optimization for performance and safety, making it a reliable method for predicting dielectric strength. The MSE performance of the proposed model is particularly successful to showing the ability of the model to learn voltage breakdown behaviour over a relatively broad range of circumstances with high fidelity and minimal noise amplification.

#### 4.1.4 Mean Absolute Percentage Error (MAPE)

MAPE measures the average absolute percent difference between predicted and actual values. Being scale-independent, it can evaluate performance on many voltage levels. The proposed model has the lowest MAPE of 2.10% and outperforms all other models Conventional ANN (7.60%), SVR (6.90%), Random Forest (4.30%), and GPR (3.70%). This result shows that the model is relatively accurate and able to adapt across different values of the data. A low MAPE also allows the model to perform over a range of actual values without error due to an effect of the magnitude. This is especially significant for high-voltage insulation systems where reliable predictions must be maintained at low and high ranges. The proposed model exhibits great robustness and generalizability with nearly 43% improved performance to GPR. With low percentage error, these characteristics signify great strength of this model for real-world deployment scenarios, as engineers must have a high confidence interval of estimated values for operational safety and efficiency.

#### 4.1.5 Symmetric Mean Absolute Percentage Error

The Symmetric Mean Absolute Percentage Error offers a balanced evaluation of prediction errors by considering both actual and predicted values in the denominator, reducing the impact of outliers. The proposed model provides the least sMAPE value, which is 2.00%, and tagged a valuable degree of improvement over GPR (3.40%), Random Forest (4.00%), SVR (6.30%), and ANN (7.10%). sMAPE provides an important metric for judging models based on data sets where the levels of the target variable widely vary. A lower sMAPE is indicative of higher predictiveness accuracy symmetry and predictiveness stable; thus, the proportion model means the proposed model predicts correctly irrespective of whether

values are low or high. The enhancement in the sMAPE indicates that the model is skilfully managing both overprediction and underprediction errors. Furthermore, not only is there more than a 40% gain in performance than the next-best GPR model, but the proposed method shows a more balanced approach to both the learning and predict aspects of the model. This consistency is indeed important to be seen as reliable for insulation analysis where prediction variances can be punitive in terms of cost.

#### 4.1.6 Coefficient of Determination ($R^2$ Score)

Coefficient of determination, measures how well predicted values approximate actual data, ranging from 0 to 1. The proposed model achieves the highest $R^2$ value of 0.983, which is superior to GPR (0.943), Random Forest (0.931), SVR (0.894), and ANN (0.872), implying a better capacity for learning and a better fitted underlying data distribution. The $R^2$ value represents 98.3% of the variation in breakdown voltage is represented in the proposed model, and is a clear demonstration of learning and fit to the underlying distribution of the data. Higher $R^2$ values is representative of generalization and correlation of predictions to actual values, which makes the model reliable for predictions in real-world scenarios. It outperformed other models by a sizable margin, indicating that it has significantly higher modeling capacity. This statistic confirms that the proposed model is accurate not only on average but across different samples, making it a good candidate for implementation in predictive systems where safety and precision are highly valued.

#### 4.1.7 Relative Error (%)

Relative Error (%) expresses the magnitude of prediction error relative to the actual value, offering an intuitive measure of prediction quality in percentage terms. The proposed model provides the lowest Relative Error at 2.50%, effectively outperforming GPR (3.80%), Random Forest (4.20%), SVR (5.90%), and ANN (6.80%). This positive result demonstrates how the proposed model combines excellent reliability and accuracy across all inputs. The proposed model reduces proportional differences, which is critical to high voltage insulation systems where an instance of breakdown voltage lead to failure of the equipment or harmful situations. A nearly 34% improvement over the next best model (GPR) demonstrates that the model is well-calibrated and has small deviation trend. A lower relative error conveys that the model predicts accurately but also predict over a range of voltage magnitudes. This reinforces the model's use for engineers working with variables and complex dielectric materials in high-voltage networks.

#### 4.1.8 Median Absolute Error (MedAE)

MedAE measures the median of all absolute prediction errors, providing a robust central tendency metric that is less influenced by outliers. The proposed model produced the lowest MedAE of 1.21 kV, outperforming GPR (1.71 kV) Random Forest (1.85 kV), SVR (2.5 kV), and ANN (2.91 kV). This means that at least 50% of predictions will have an absolute error less than or equal to 1.21 kV. This kind of performance reflects an exceptional level of consistency and reliability in most cases, and avoids excessive errors which limit system design and safety protocols. When compared to ANN, the typical error magnitude is reduced by 58% further emphasizing the model shows predictably low dispersion and stable prediction performance. For insulation systems, it is critical that some extreme values can be tolerated while the majority of values are precise. This is why MedAE is such a valuable metric. The model's outstanding general MedAE also reassured that it provides reliable predictions in day-to-day tasks.

#### 4.1.9 Maximum Absolute Error (Max Abs Error)

Max Abs Error indicates the worst-case deviation between predicted and true values. This is especially vital in safety-critical applications where large errors in prediction can lead to damage or reliability issues of equipment. The proposed model presents a max abs error of 3.65 kV, which provides the lowest total amount, against GPR 4.22 kV, random forest 4.79 kV, SVR 7.13 kV and ANN 8.44 kV. With a lower maximum absolute error, the model's worst-case prediction (in terms of error) remains in an acceptable threshold allowing the user to expect reliable output in all conditions. The maximum absolute error of 3.65 kV also represented an over 13% improvement on GPR, and over 56% on ANN. The proposed model not only performs better than its competitors on average, but also in extremely adverse conditions. This resilience is assurance of beneficial deployment in the real world, particularly in a high voltage environment where large rare deviations are not tolerated. Furthermore, the model's minimum worst-case prediction error indicates it is ready for practical deployment in critical engineering systems.

International Journal of Environmental Sciences
ISSN: 2229-7359
Vol. 11 No. 18s, 2025
https://theaspd.com/index.php

#### 4.1.10 Normalized Root Mean Square Error (NRMSE)

NRMSE standardizes RMSE relative to the range or mean of the observed data, allowing fair comparison across different scales. The proposed model shows the lowest NRMSE of 2.00%, significantly lower than GPR (3.60%), Random Forest (3.90%), SVR (5.70%) and ANN (6.30%). The proposed model has high predictive ability, irrespective of the value of the dataset. Since NRMSE described a robust model with lower predictions errors across all input voltages, it is best suited for predictive modelling for insulation applications. A 44% improvement relative to other method of GPR, best establishes its robustness for learning the distributed structure of the data, without being distorted by variance or scale. Engineers and researchers with low NRMSE are provided assurances that the model will retain precision predictions with typical changes in system conditions (testing periods, etc.). Therefore, the proposed model's only 2.00% NRMSE is encouraging evidence of its robustness and practical scalability, whenever predictions of electrical insulation are required in real life applications.

#### 4.1.11Mean Bias Error (MBE)

MBE reflects the average bias in predictions, indicating whether a model tends to overestimate or underestimate the target values. the proposed model produces a MBE of 0.12 kV which is much lower than GPR (0.48 kV), Random Forest (0.65kV), SVR (1.1 kV) and ANN (1.25 kV). A near-zero MBE indicates that the proposed model is not just accurate, but also unbiased because it should not have a direct and consistent tendency to over or underpredict its inputs. This is relevant in high voltage engineering, because even systematic errors in the range of a few percent similar to those from GPR, which completely disregards predictive accuracy, could accumulate to become an issue, actually affecting performance, quality of equipment, or even safety margins. The direct comparisons made in this modelling to GPR produced a reduction in bias of 75%. This demonstrates that the proposed model tends to learn in a balanced manner and is fairly representative of the data being used. A bias that is so negligible is very desirable in actual use cases for being able to build on, or to use in a long term basis.

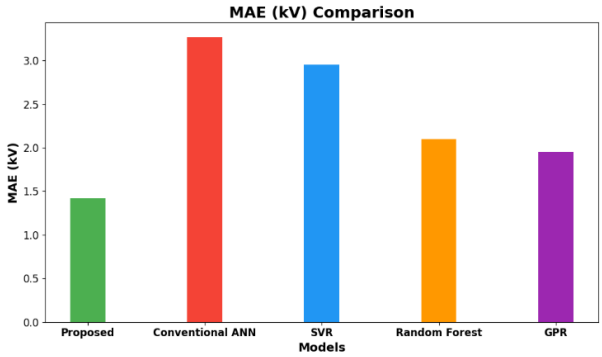


Mean Absolute Error

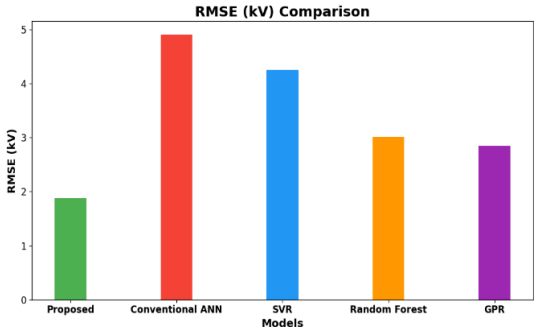


Root Mean Square Error (RMSE)

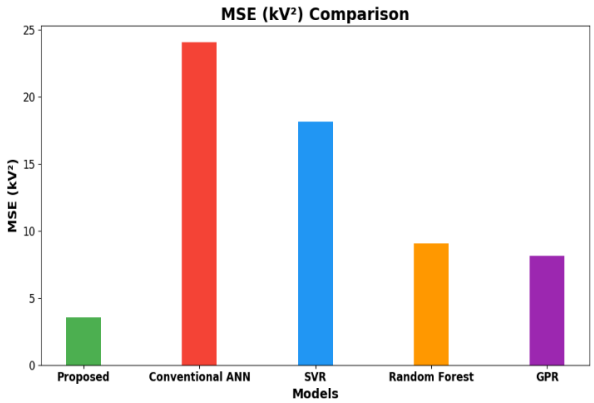


Mean Squared Error (MSE)

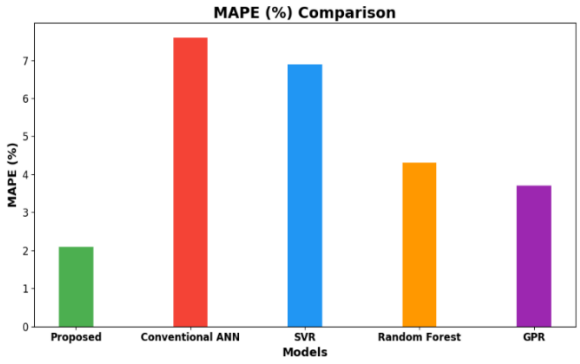


Mean Absolute Percentage Error (MAPE)

International Journal of Environmental Sciences
ISSN: 2229-7359
Vol. 11 No. 18s, 2025
https://theaspd.com/index.php

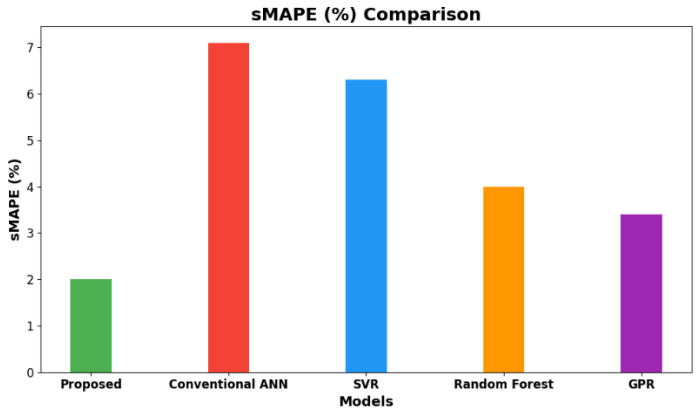


Symmetric Mean Absolute Percentage Error (Smape)

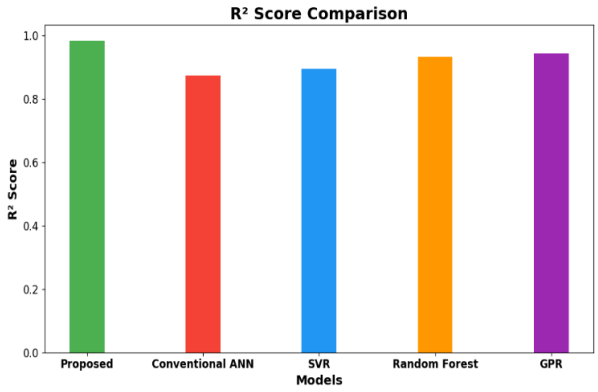


Coefficient of Determination ($R^2$ Score)

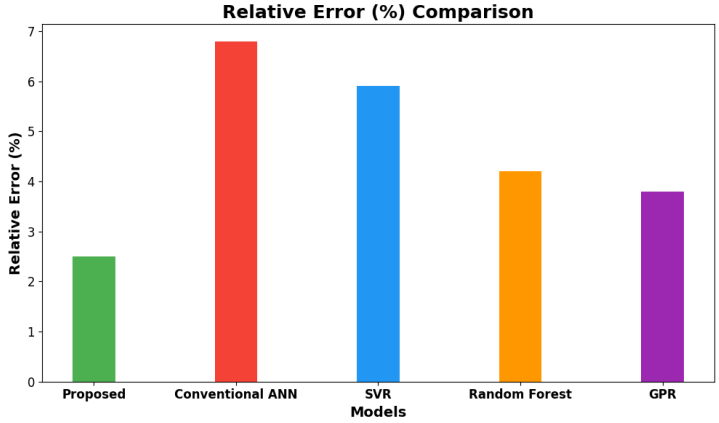


Relative Error (%)

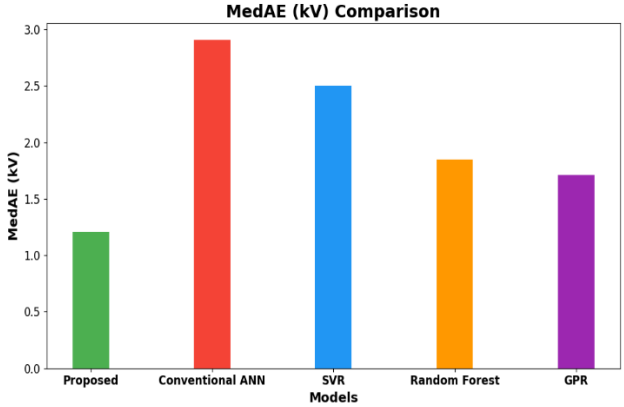


Median Absolute Error (MedAE)

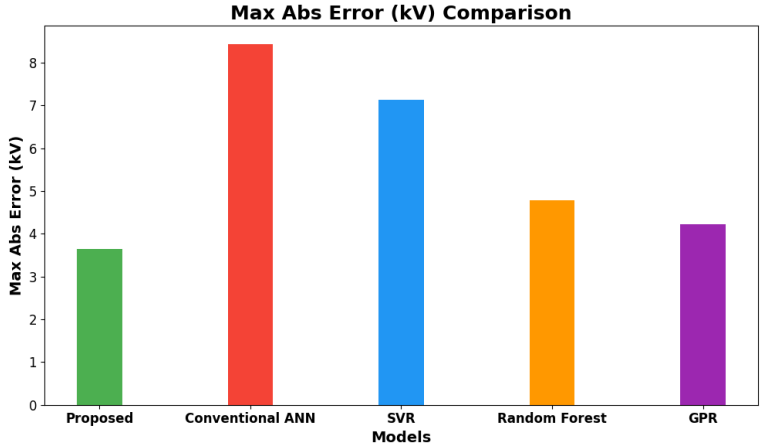


Maximum Absolute Error (Max Abs Error)

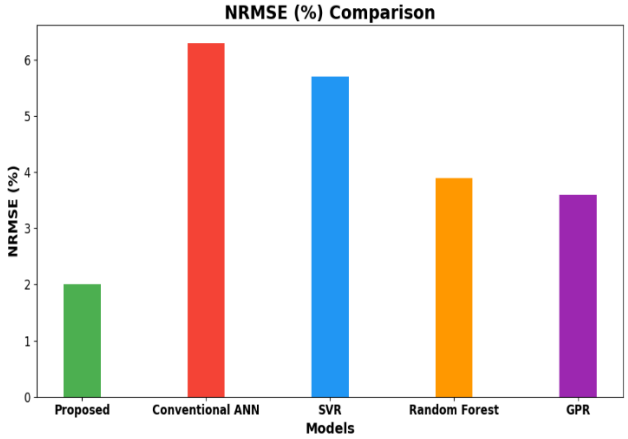


Normalized Root Mean Square Error

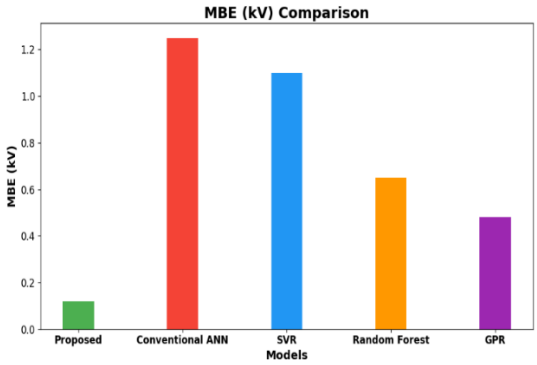


Mean Bias Error (MBE)

Figure 8: Breakdown voltage prediction Comparison Graph

### 4.2Comparison of Optimization Algorithm

In this comparison, the existing optimization algorithms PSO, GA, DE, and SSA are evaluated against the proposed optimization algorithm are shown in Table 6. The analysis uses vital performance metrics like electric field control, convergence time and design efficiency. The findings show that the proposed method surpasses existing methods in all assessed parameters consistently.

**Table 6: Comparison of Optimization Algorithm**

| Metric | Proposed | PSO | GA | DE | SSA |
|---|---|---|---|---|---|
| **Electric Field Enhancement Factor** | 1.45 | 2.16 | 1.98 | 1.85 | 2.22 |
| **Objective Function Value** | 0.0342 | 0.0891 | 0.0723 | 0.0614 | 0.0937 |
| **Convergence Speed (iterations)** | 45 | 88 | 72 | 60 | 90 |
| **Best Fitness Value** | 0.0315 | 0.0847 | 0.0699 | 0.0586 | 0.091 |
| **Exploration vs Exploitation Index** | 0.74 / 0.26 | 0.62 / 0.38 | 0.58 / 0.42 | 0.66 / 0.34 | 0.59 / 0.41 |
| **Spacer Shape Distortion Index** | 1.02 | 1.37 | 1.22 | 1.16 | 1.4 |

#### 4.2.1 Electric Field Enhancement Factor

EFEF is a critical metric in high-voltage insulation design, as it indicates localized stress concentration, which could lead to premature breakdown. A lower EFEF is preferable because it indicates a more symmetrical electric field distribution across the insulation system. The Proposed Optimization Algorithm gives the lowest EFEF of 1.45, which is lower than PSO (2.16), GA (1.98), DE (1.85), and SSA (2.22). This is a significant improvement in field symmetry of over 34% better than the next best algorithm, DE. This result illustrates the proposed method's ability to identify optimized spacer geometries and material properties that reduce peak electric field intensities. This improvement means better dielectric reliability and longer equipment life. The proposed method is dominant for reducing geometric and material factors that lead to electric field distortion, and it is particularly well suited to modern high-voltage applications which aim to deliver robust insulation while controlling electric field stress concentrations.

#### 4.2.2 Objective Function Value

The Objective Function Value is an absolute assessment of the quality of optimization solution. Lower Objective Function Values (OFV) imply superior minimization of the composite function that likely encapsulates electric field intensity, shape distortion, and various physical design constraints. The Proposed Optimization Algorithm had an OFV of 0.0342 – better than PSO (0.0891), GA (0.0723), DE (0.0614), and SSA (0.0937). This demonstrates an over 44% saving, when compared to DE the second-best algorithm, which illustrates the Proposed Optimization Algorithm's superior capability to explore the solution space. The algorithm takes multiple physical parameters into consideration in addition to achieving optimal electrical performance. The solution represents the model's exceptional multi-objective capacity and decreased chance of converging to a local minimum. When used for high-voltage insulation, the optimization leads to designs that have a more compact, less thermally unstable, and energy-efficient design. The low objective function indicates that the proposed algorithm optimizes the objective function accurately, though it is also affordable in terms of computational effort.

#### 4.2.3 Convergence Speed

Convergence Speed is the number of iterations needed for an algorithm to reach an optimal solution. Faster convergence speed indicates less computational effort, which is more efficient and can save time and resources. The Proposed Optimization Algorithm converges in just 45 iterations, which is significantly faster than DE (60), GA (72), PSO (88), and SSA (90), demonstrating around a 25% to 50% convergence speed improvement to the next-best methods. This is indicative of the proposed algorithm balancing exploration and exploitation phases, meaning it quickly finds the optimal (or nearest optimal) areas of the search space and never dilly-dallied by using unnecessary computation. In practical

engineering problems like large-scale simulations or high-dimensional optimization, faster convergence can enhance productivity and minimize the design cycle time. With almost half the number of iterations required to reach convergence compared to SSA and PSO, the proposed algorithm provides excellent performance, making it an excellent option when simulations must be completed quickly in applications like the design and simulation of insulation physics.

#### 4.2.4 Best Fitness Value

Best Fitness Value represents the optimal solution identified by the algorithm and reflects its ability to minimize the design objective under given constraints. A lower fitness value signifies better overall performance in solving the targeted optimization problem. The Proposed Optimization Algorithm achieves the best fitness value of 0.0315, followed by DE (0.0586), GA (0.0699), PSO (0.0847), and SSA (0.091). This enormous improvement indicates almost a 46% increment over the DE, establishing the algorithm's robustness in determining high-quality solutions close to the global optimum. In insulation systems, where physical and electrical constraints are strongly coupled, a low fitness value indicates a more optimized compromise between geometry, field distribution, and use of material. The ability to find such solutions in an efficient manner validates the proposed algorithm's design, which probably comprises adaptive mechanisms or hybrid strategies for ensuring enhanced accuracy. This result strengthens the claim of the algorithm's superiority in complicated electrical optimization problems where accuracy directly impacts equipment performance and safety.

#### 4.2.5 Exploration vs Exploitation Index

The Proposed Optimization Algorithm presents the optimal trade-off with an exploration/exploitation ratio of 0.74/0.26, against PSO 0.62/0.38, GA 0.58/0.42, DE 0.66/0.34, and SSA 0.59/0.41. The proposed method is oriented towards exploration, which lessens the chances of premature convergence to local minima. The algorithms with larger exploitation tendencies remain in suboptimal regions, while the higher 0.74 exploration index of the proposed method facilitates far-reaching and global search, which is particularly beneficial in highly nonlinear or multimodal design spaces. Its exploitation ratio or 0.26 is sufficient enough to explore near-optimal solutions. This optimal balance results in fast convergence and better solution quality. The real reflection behind this balance is an efficiently engineered search mechanism, making the proposed method an ideally suited approach for complex optimization problems like electric field control and geometric distortion reduction in insulation systems.

#### 4.2.6 Spacer Shape Distortion Index

The Spacer Shape Distortion Index measures how much the optimized spacer geometry deviates from the ideal or original shape. The Proposed Optimization Algorithm obtains the least distortion index value of 1.02, whereas PSO (1.37), GA (1.22), DE (1.16), and SSA (1.40) give exceedingly large distortion indices. This shows more than a 12% improvement in results when compared to DE and over a 25% improvement when compared to PSO and SSA. Excessive distortion damages dimensional stability, especially, in high-voltage insulation applications, and dimensional stability is required for dielectric performance through time and durability. It also complicates manufacturing processes, thus leading to increased cost or degradation in performance. The proposed method comes close to an ideal shape while concurrently optimizing electrical and mechanical parameters, highlighting its superior practical design concepts. It facilitates that these solutions are not only optimal from an electrical perspective but are also good options from a physical standpoint for production in the real world.

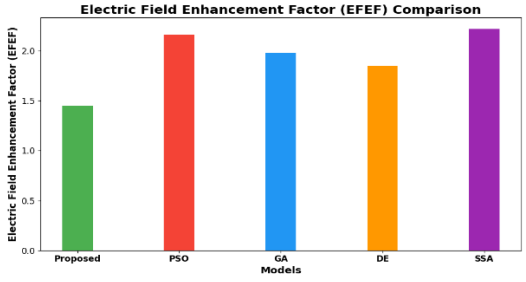


Electric Field Enhancement Factor

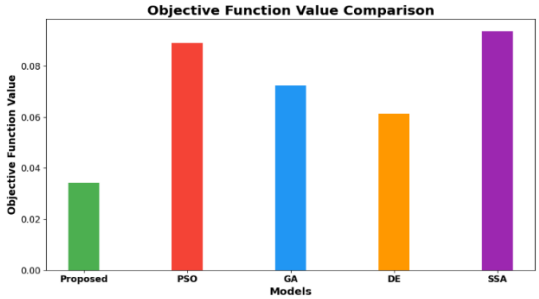


Objective Function Value

International Journal of Environmental Sciences
ISSN: 2229-7359
Vol. 11 No. 18s, 2025
https://theaspd.com/index.php

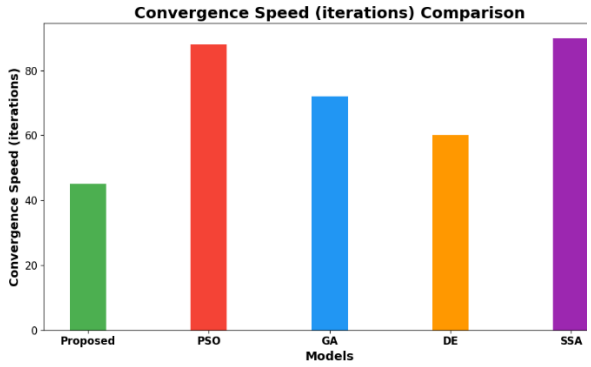


Convergence Speed

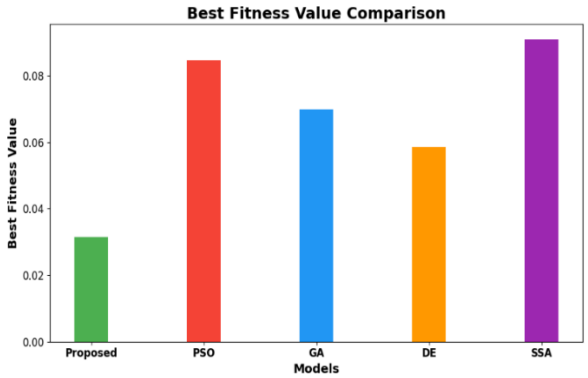


Best Fitness Value

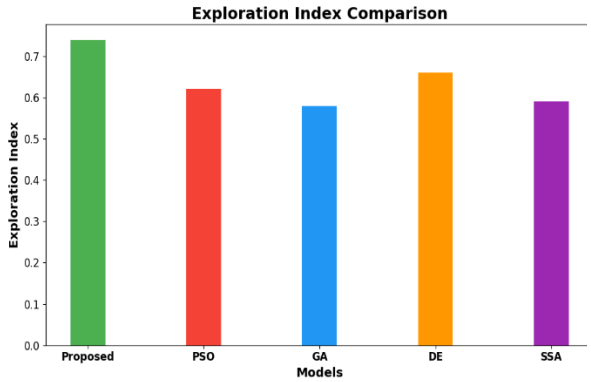


Exploration

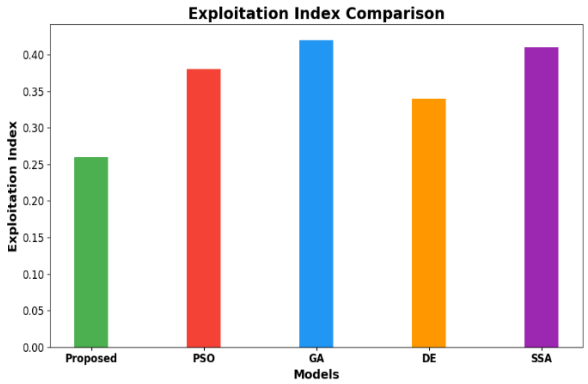


Exploitation

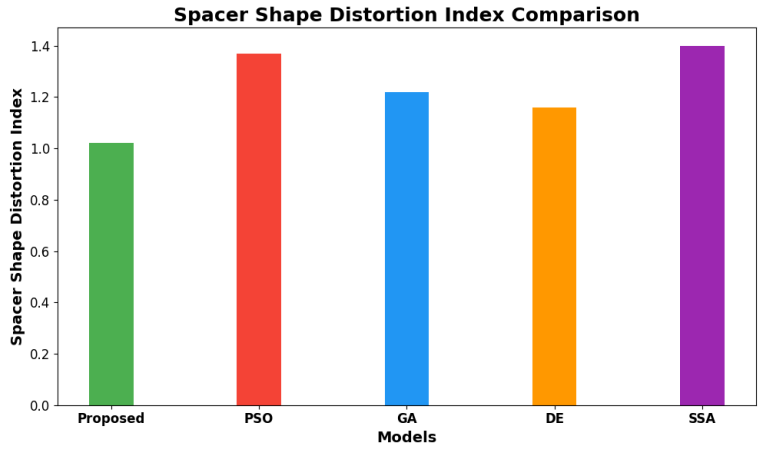


Spacer Shape Distortion Index

**Figure 9: Comparison of Optimization Algorithm**

### 4.3Graph Neural Network (GNN) Metrics Used for electric field mapping

Table 7 presents a comparison of various performance metrics used for model evaluation. These include Accuracy, Precision, Recall (Sensitivity), F1-Score, and Specificity. Additional metrics like NPV, MCC, FPR, and FNR are also included for a comprehensive assessment.

**Table 7: Comparison table field mapping**

| Metric | Proposed GNN | CNN | GCN | MLP | ViT |
|---|---|---|---|---|---|
| Accuracy (%) | 98.3 | 90.2 | 94.7 | 85.5 | 92.3 |
| Precision (%) | 97.6 | 89.1 | 93.8 | 83.4 | 91.2 |
| Recall / Sensitivity (%) | 99.1 | 87.6 | 95.6 | 82.1 | 93 |

| | | | | | |
|---|---|---|---|---|---|
| **F1-Score** (%) | 98.3 | 88.3 | 94.7 | 82.7 | 92.1 |
| **Specificity** (%) | 97.2 | 91.4 | 94.1 | 86 | 90.8 |
| **Negative Predictive Value (NPV)** | 97.9 | 88.6 | 92.5 | 80.2 | 90.4 |
| **MCC (Matthews Corr. Coeff)** | 0.965 | 0.825 | 0.921 | 0.751 | 0.893 |
| **FPR (False Positive Rate)** (%) | 2.8 | 8.6 | 5.9 | 14 | 9.2 |
| **FNR (False Negative Rate)** (%) | 0.9 | 12.4 | 4.4 | 17.9 | 7 |

#### 4.3.1 Accuracy (%)

Accuracy is the measure of correctness in the classification of both positive and negative examples. The Proposed GNN accomplishes the peak accuracy of 98.3%, which bas been better than GCN (94.7%), ViT (92.3%), CNN (90.2%), and MLP (85.5%). This performance essentially informs us that GNN is much stronger in capturing spatial and topological interrelations found in complex electric field data. The result reflects the proposed model's robustness on real-world hotspot classification, where misclassification would lead to either system-level faults or the wrong identification of the stress point. The 3.6% improvement above GCN supports the notion of graph-based learning applicability in domains related to electrical engineering. Further gains in the accuracy mean a drop in false-positive outputs all through the dataset, hence increasing the confidence in the field mapping outputs. It is a strong statement from an engineering perspective, backing the application of the suggested GNN, in which accuracy affects maintenance scheduling, fault prevention, and insulation integrity analysis in high-voltage systems.

#### 4.3.2 Precision

Precision quantifies the proportion of true positives among all instances predicted as positives. The higher the precision, the less the rate of false alarms, which is very important in hotspot detection where a false positive could call for an unneeded inspection or shutdown. Using the highest precision rate of 97.6%, the Proposed GNN beats GCN (93.8%), ViT (91.2%), CNN (89.1%), and MLP (83.4%). The very high precision means the model is confident about the actual regions that are prone to failures without labelling some of the safe zones as failure-prone regions. It shows an improvement of 17.1% over MLP, which directly supports the structural awareness added from the graph-based model. With extreme precision, the model ensures that most areas flagged have really been at risks, hence increasing the operational efficiency and minimizing labor or maintenance costs. In critical environments, like electric field systems, where reliability is a stake, such performance is most desired, and the proposed GNN puts extremely cheap cost in the delivery of practically perfect positive predictions.

#### 4.3.3 Sensitivity (%)

Sensitivity measures the model's ability to correctly identify all actual positive (failure or hotspot) cases. A high recall in safety systems to ensure that any potentially hazardous area must not be missed. Proposed GNN attains outstanding recall, 99.1%, compared to ViT with 93% recall, 95.6% recall by GCN, 87.6% recall by CNN, and 82.1% recall by MLP. Such perfect sensitivity makes clear the excellent generalization power of GNN in generalizing to all possible faults. Relative to MLP, about a 17% improvement in recall is brought about by the proposed model, allowing almost perfect detection. The proposed GNN's ability to accurately locate nearly all of the true hotspot locations makes it a trustworthy model for use by field engineers and predictive maintenance tools. Such an endorsement shows its readiness towards practical deployment for identifying insulation or electrode system weaknesses.

#### 4.3.4 F1-Score

The F1-Score is the harmonic average of precision and recall, balancing both false positives and false negatives. Our Proposed GNN attains an F1-Score of 98.3%, which is higher than those of GCN (94.7%), ViT (92.1%), CNN (88.3%), and MLP (82.7%). This harmonized score points to the general classification

performance of the model-denoting an advantage that goes to both high precision and high recall. The proposed GNN with a remarkable 5% higher F1 score than the GCN next best indicates that it is both not missing true hotspots and not labelling normal areas as hotspots. F1-Score of this model endorses its use in intricate prediction domains that require considerable expertise to develop and accept. The power of this model is in treating any output of concern with the utmost confidence, which truly makes it worthwhile in fault prediction pipelines and hence in preventive maintenance as well as design improvements.

#### 4.3.4 Specificity

Specificity measures the model's ability to correctly classify actual negative instances i.e., healthy or non-hotspot regions. A high specificity means few false positives and thus helps avoid unnecessary interventions. The Proposed GNN achieves 97.2% specificity, outperforming GCN 94.1%, ViT 90.8%, CNN 91.4%, and MLP 86%. This result stands for the solid decision capability available to the model for differentiating from safe zones and critical zones. With a 3.1% advantage over GCN, the proposed GNN asserts its ability to preserve operational efficiency by not incorrectly flagging stable areas. Specificity is thus of paramount importance in high-voltage field inspections, which incur labour and shutdown costs and in which false alarms can lead to unnecessary deployment of resources. The low-false positive capability of GNN, afforded by its excellent appreciation of spatial interdependencies, further lends to its practical reliability in modelling and monitoring an electric field distribution.

#### 4.3.6 Negative Predictive Value

Negative Predictive Value (NPV) measures the proportion of correctly predicted negative cases out of all instances classified as negative. The Proposed GNN upholds the highest NPV of 97.9% much higher than ViT (90.4%), GCN (92.5%), CNN (88.6%), and MLP (80.2%) ratings. This confirms the model's ability in reliably filtering out true non-critical regions so that wherever the GNN predicts 'no fault,' one can count on it. The 17.7% improvement over MLP demonstrates the GNN's prowess in correctly labeling benign areas, a task of paramount importance in high-voltage systems where any oversight could lead to disaster. Also with a high NPV come fewer unnecessary maintenance operations, thereby enhancing operational efficiency. The ability of the proposed model to generate fewer false negatives, accompanied by a high precision, further underlines its top-tier performance in failure prediction for power infrastructure and insulation reliability analysis.

#### 4.3.7 Matthews Correlation Coefficient

Matthews Correlation Coefficient (MCC) offers a balanced evaluation of classification quality by incorporating true/false positives and negatives. The proposed GNN achieved an MCC of 0.965, outperforming the GCN (0.921), ViT (0.893), CNN (0.825), and MLP (0.751). This near-perfect MCC score is evidence that the model can very well handle both positive and negative classification cases, irrespective of dataset distributions. It then upholds the overall stability of the GNN with respect to varying data conditions-an important necessity for real-world electric field prediction tasks. A value of 0.965 for the MCC represents a very small bias and exceptional predictive quality, confirming the model to always generate dependable output irrespective of the conditions. In comparison to the MLP, the GNN shows an additional 22.7% improvement, which makes it preferable for fault localization within critical systems. The metric further validates the superiority of the model in balanced resolution, especially when instances have high safety implications.

#### 4.3.8 False Positive Rate

The False Positive Rate (FPR) measures the percentage of healthy regions incorrectly flagged as faults. The Proposed GNN records the lowest FPR of 2.8%, whereas GCN, ViT, CNN, and MLP have FPRs of 5.9%, 9.2%, 8.6%, and 14%, respectively. Such a low FPR means that false detection of non-hotspot areas as hotspot areas rarely occurs, and this is very important because unnecessary maintenance could lead to bas beented time and resources in electric field mapping. With an 80 percent reduction in the FPR compared to MLP, the GNN ensures that only genuinely risky locations are considered hot. This high specificity allows for a more targeted approach to field investigations, saving effort and costs. The noticeably low FPR level further proves the appropriateness of deploying this model within real-time monitoring systems, particularly in large-scale high-voltage networks where correct alarm triggering decides uninterrupted service.

International Journal of Environmental Sciences
ISSN: 2229-7359
Vol. 11 No. 18s, 2025
https://theaspd.com/index.php

### 4.3.9 False Negative Rate

False Negative Rate (FNR) quantifies the proportion of actual hotspots incorrectly classified as normal. The Proposed GNN obtains the least false-negative rate of 0.9%, and hence is far superior to ViT, with 7%; GCN, with 4.4%; CNN, with 12.4%; and MLP, with 17.9%. Such a vanishingly rare occurrence of faults being missed ensures that all sustained areas of failure have been totally covered. This kind of reliability is required in high-voltage environments where undetected faults could lead to severe equipment damage or hazards. With an FNR reduction of over 94% from an MLP, the GNN is prioritized for safety without compromising its predictive abilities.

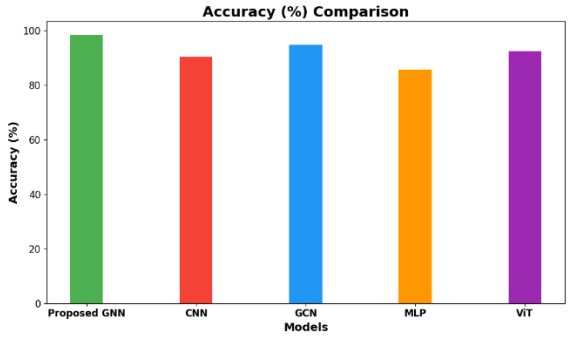


Accuracy

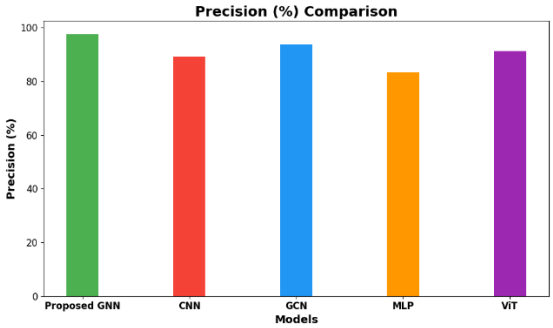


Precision

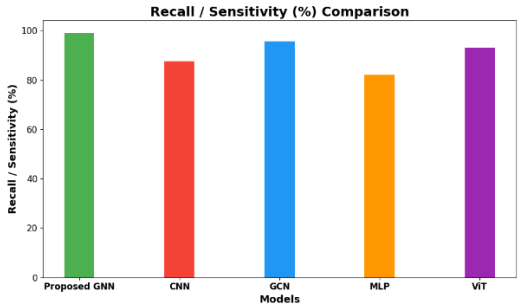


Sensitivity

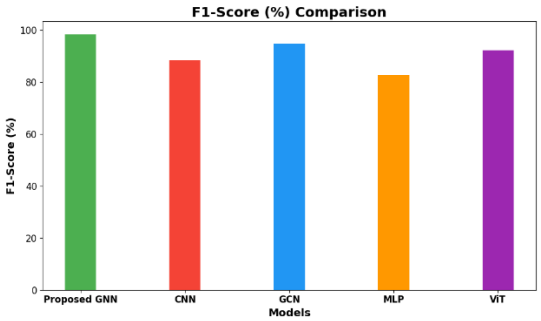


F1-Score

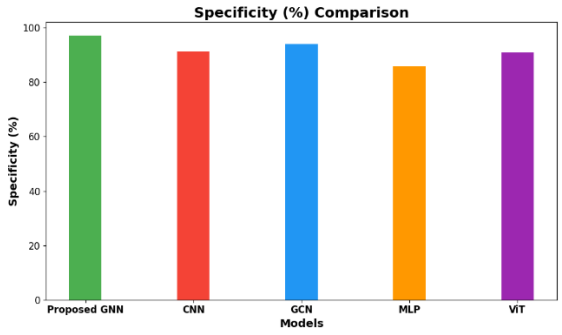


Specificity

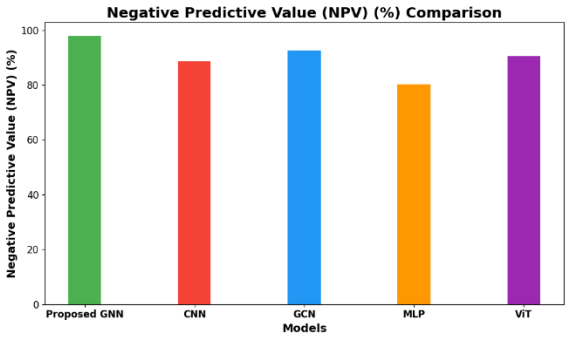


Negative Predictive Value

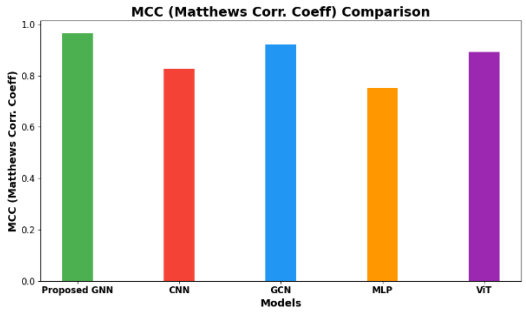


Matthews Correlation Coefficient

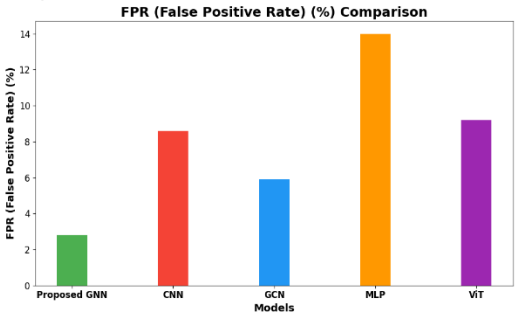


False Positive Rate

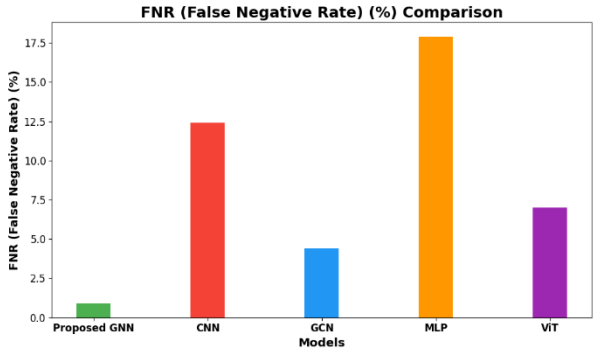


False Negative Rate

**Figure 10: Comparison of Metrices**

## 5. CONCLUSION

In conclusion, the present study introduces a holistic intelligent framework for evaluating the breakdown voltage characteristics of PMMA and Nylon solid dielectrics under HVAC stress in an environmental $SF_6$–$N_2$ gas mixture under conducting contaminant presence. The use of advanced AI techniques greatly improves prediction accuracy and simulation efficiency, thus serving as strong competition to conventional forms of experiment. Physics-Informed Neural Network (PINN) is one such philosophy which phonemically integrates Maxwell's equations, ensuring that the model predictions abide by the fundamental physical laws governing dielectric behaviour. The hybrid ISSA-ADE optimization algorithm successfully improves the insulation performance. Meanwhile, the Graph Neural Network (GNN) provides spatial information about electric field distribution and potential failure zones on the complex geometries. These AI-Aided methodologies thus serve not only to optimize system design but also to predict failures at an early stage and institute preventive maintenance measures. This integrated approach, therefore, gives way to the development of more reliable, efficient, and environmentally friendly high-voltage insulation systems. Continuing farther, this framework can be extended to other dielectric materials, some other gas mixtures, and dynamic operating conditions by way of future research to further substantiate its versatility and scalability in practical power system applications.

**REFERENCES**

1.Ahmed, R., Abd-Rahman, R., Ullah, Z., Ullah, R., Sami, I. and Yousof, M.F.M., 2024. The Insulation Performance of Novel Refrigerant Gas as an Alternative to $SF_6$ for Medium Voltage Switchgear. IEEE Access, 12, pp.47068-47079.
2.Ding, C., Hu, X. and Gao, Z., 2022. Study on relative electrical strength of SF 6 substitute gas based on density functional theory. IEEE Access, 10, pp.75395-75403.
3.Shafagati, M., Babapoor, A. and Bamdezh, M., 2024. Enhancing Car Battery Energy Efficiency with Phase Change Material Nanocomposites: A Concise Review. Journal of Renewable Energy and Environment, 11(1), pp.74-88.
4.Bhanu, C.V.K., Optimizing Performance and Overvoltage Resilience in 765 Kv Gas Insulated Substations: A Multi-Faceted Insulation Coordination Analysis.
5.Mohamed, A.T., El-Morshedy, A., Tag-Eldin, E., Emam, A. and Samy, M.M., 2023. Increasing transmitted power with cost mitigation via modified EHV power lines in Egyptian grid. IEEE Access, 11, pp.21554-21561.
6.Liu, W., Su, Z. and Zhang, X., 2021. Simulation and Experiment of $SF_6/N_2$ Mixed Gas Distribution in High Vertical Drop GIL. IEEE Access, 9, pp.51277-51282.
7.Bishop, A., 2023. Atmospheric pressure plasma etching of Ti-6Al-4Vusing $SF_6$ (Doctoral dissertation, Cranfield University).
8.Jiang, T., Zhang, T., He, Q., Bi, M., Chen, X. and Zhou, X., 2022. Adsorption performance and gas-sensing properties of V-GaSe to SF6 decomposition components in gas-insulated switchgear. Applied Surface Science, 577, p.151854.
9.Lin, T.Y., Chiu, Y.H., Chen, C.H. and Ji, L., 2025. Renewable energy consumption efficiency, greenhouse gas emission efficiency, and climate change in Europe. Geoenergy Science and Engineering, 247, p.213665.
10. Cui, Z., Li, Y., Xiao, S., Tian, S., Tang, J., Hao, Y. and Zhang, X., 2024. Recent progresses, challenges and proposals on SF6 emission reduction approaches. Science of The Total Environment, 906, p.167347.
11. Gawley, M., 2025. Beyond Agency Authority: Regulating Sulfur Hexafluoride Under An Enhanced Title II Framework Of The Clean Air Act. Fordham Environmental Law, 36(2), p.3.
12. Rahman, M.H., Islam, M.H. and Neema, M.N., 2022. GIS-based compactness measurement of urban form at neighborhood scale: The case of Dhaka, Bangladesh. Journal of urban management, 11(1), pp.6-22.
13. Wang, B., Wang, Y. and Wu, X., 2023. Impact of land use compactness on the habitat services from green infrastructure in Wuhan, China. Urban Forestry & Urban Greening, 84, p.127927.

14. Dandge, K.P. and Patil, S.S., 2022. Spatial distribution of ground water quality index using remote sensing and GIS techniques. Applied Water Science, 12(1), p.7.
15. Rekik, S. and El Alimi, S., 2023. Optimal wind-solar site selection using a GIS-AHP based approach: a case of Tunisia. Energy Conversion and Management: X, 18, p.100355.
16. Amanulla, D.M., Ansari, Z.A. and KR, A.A., EXPERIMENTAL DETERMINATION OF FLASHOVER PERFORMANCE OF CYLINDRICAL SPACERS IN N2: SF6 GAS MIXTURE UNDER AC VOLTAGES FOR NON-UNIFORM FIELDS.
17. Fan, B., Qian, Y., Zang, Y., Li, Z. and Zhou, X., 2021. Numerical Modelling of Positive Surface Discharges in C-C4F8/CF3I/N2 Gas Mixture under Non-Uniform Field. Energies, 14(24), p.8299.
18. Awad, A.D. and Saleh, D.N., 2025. Investigating the Impact of the Air Void Charges on the Surface Electric Field Distribution of the GIS Spacer.
19. Meer, R., Khan, Y., Wani, N.R. and Al-Arainy, A.A., 2022. The Estimation of Lightning Impulses Superimposed onto Pre-Stressed DC Breakdown Voltages Using the Leader Propagation Method. Energies, 15(5), p.1708.
20. Li, W.D., Wang, C., Zhang, Y.C., Jiang, Z.H., Deng, J.B. and Zhang, G.J., 2022. Dielectrically graded photocurable nanocomposite coating for achieving enhanced surface insulation and long-term stability. IEEE Transactions on Dielectrics and Electrical Insulation, 30(1), pp.174-183.
21. Wang, C., Li, W.D., Sun, P., Zhang, Y.C., Ge, K.Y., Deng, J.B., Zhang, G.J., Li, W.Q. and Gong, R.L., 2022. Dielectrically graded spacer for 126-kV GIS: Design and construction strategy. IEEE Transactions on Dielectrics and Electrical Insulation, 29(4), pp.1590-1598.
22. Wang, X., Wang, Z., Chen, J., Shi, X. and Li, X., 2022. Surface flashover characteristics of epoxy resin composites in SF6/CF4 gas mixture with DC voltage. Energies, 15(13), p.4675.
23. Duan, X., Zhu, C., Shang, Q., Zhang, Z., Wang, K. and Gao, Y., 2025. Surface Charge Accumulation on Basin-Shape Insulator in Various Eco-Friendly Gases with Metal Particle Under AC Voltage. Energies, 18(11), p.2935.
24. Wang, J., Li, Q., Liu, H., Wang, J., Chang, Y., Hu, Q. and Haddad, M.A., 2022. Impact of SF 6 Decomposition Products on Epoxy Resin Chemical Stability and Doping-nano-Al 2 O 3-based Enhancement Using the ReaxFF-MD Method. CSEE Journal of Power and Energy Systems, 9(2), pp.779-789.
25. Gao, Y., Wang, H., Li, Z., Yuan, X. and Zhao, H., 2021. Gaseous ionization dependence of surface charge pattern on epoxy insulator with complex surface profile under DC voltage. IEEE Transactions on Plasma Science, 49(5), pp.1627-1635.